Electronic supplementary information (ESI) for

Bismuth Phosphate Nanoparticle Catalyst for Direct Oxidation of Methane into Formaldehyde

Aoi Matsuda,[a] Kazuhiko Obara,[a] Atsushi Ishikawa,[b] Meng-Hsuan Tsai, Chia-Hsin Wang, Yu-Chuan Lin,[d] Michikazu Hara,[a] Keigo Kamata*[a]

[a]Laboratory for Materials and Structures, Institute of Innovative Research, Tokyo Institute of Technology, 4259 Nagatsuta-cho, Midori-ku, Yokohama, Kanagawa 226-8503, Japan

[b] Department of Transdisciplinary Science and Engineering, School of Environment and Society, Tokyo Institute of Technology, 2-12-1 Ookayama, Meguro-ku, Tokyo 152-8550, Japan

[c] National Synchrotron Radiation Research Center, 101 Hsin-Ann Rd, 30076, Hsinchu, Taiwan

[d]Department of Chemical Engineering, National Cheng Kung University, 1 University Rd., Tainan, 70101, Taiwan

E-mail: kamata.k.ac@m.titech.ac.jp

Experimental

Materials. Reagents such as $Bi(NO_3)_3{\cdot}5H_2O$ (Kanto Chemical), $Fe(NO_3)_3{\cdot}9H_2O$ (Kanto Chemical), α-Bi_2O_3 (Singma-Aldrich), β-Bi_2O_3 (Kanto Chemical), $(NH_4)_2HPO_4$ (Kanto Chemical), $NH_4H_2PO_4$ (Kanto Chemical), diethylene glycol (Kanto Chemical), and DL-malic acid (Kanto Chemical) were purchased and used as-received. Distilled water was produced in-house using a water purifier (Merck Millipore Elix Essential UV 3). Helium (≥99.99995%), methane (≥99.999%), oxygen (≥99.99995%), and nitrogen (≥99.99995%) were used as-received for the catalytic oxidation of methane. $FePO_4$ nanoparticles were synthesized by the sol-gel method using malic acid as reported in ref S1.

Instruments. Bulk properties of solid materials were investigated by the following procedures.[S2–S6] Samples were identified by X-ray diffraction (XRD) using a diffractometer (MiniFlex, Rigaku) with Cu Kα radiation ($\lambda = 1.5405$ Å, 40 kV–15 mA) and equipped with a high-speed 1-dimensional detector (D/teX Ultra). Data were collected in the 2θ range of 10–80° in 0.02° steps with a continuous scanning rate of 20° min^{-1}. The chemical composition was analyzed using energy dispersive X-ray fluorescence spectroscopy (ED-XRF; EDX-7000, Shimadzu). Fourier transform infrared spectra were obtained using a spectrometer (FT/IR-6100, JASCO) equipped with a diffuse reflectance attachment.

H_2 temperature-programmed reduction (H_2-TPR) profile of $FePO_4$ were measured on a chemisorption analyzer (BELCAT-A, BEL Japan) equipped with a thermal conductivity detector (TCD) to measure changes in the decrease of H_2 in the gas stream. 50 mg of sample was placed in a quartz cell and then heated from 50 to 700 °C at a rate of 5 °C min^{-1} under 5% H_2/Ar flow (50 mL min^{-1}).[S1] H_2-TPR profiles of $BiPO_4$-DEG, $BiPO_4$-HT, α-Bi_2O_3, and β-Bi_2O_3 were measured using gas chromatography (Shimadzu GC-8A) with a TCD to measure changes in the decrease of H_2 in the gas stream. 20 mg of sample was placed in a quartz reactor (6 mm inner diameter at the catalyst bed portion) and then heated from 50 to 650 °C at a rate of 5 °C min^{-1} under 5% H_2/Ar flow (20 sccm).

The surface properties of the solid materials were investigated by the following procedures.[S2–S6] The specific surface area was determined by nitrogen adsorption-desorption isotherms measured at −196 °C with an automatic surface area and porosimetry analyzer (Tristar II, Micromeritics), and the Brunauer-Emmett-Teller (BET) surface area was estimated over the relative pressure (P/P_0) range of 0.05–0.30. The sample was heated at 150 °C for 2 h under vacuum prior to the measurements, and the BET method was utilized to calculate the specific surface area. The morphology was characterized using scanning electron microscopy (SEM; S-5500, Hitachi). Transmission electron microscopy (TEM) studies were carried out using a JEOL JEM2100F transmission electron microscope operating at an accelerating voltage of 200 kV. After directly mixing Cu grids with samples, the Cu grids were collected and mounted on a stage. X-ray photoelectron spectroscopy (XPS) data were collected on a spectrometer (ESCA-3200, Shimadzu) with a standard Mg Kα source (1253.6 eV) operated at 8 kV and 30 mA. Samples were pressed into pellets and fixed on a piece of double-sided carbon tape. The binding energy was calibrated assuming the binding energy of the P 2p line to be 133.2 eV.

Procedure for IR measurements. The amounts of Lewis and Bronsted acid sites on $BiPO_4$-DEG were estimated from FT-IR measurements for pyridine-adsorbed samples at 25 °C.[S6–S8] Samples were pressed into self-supporting disks (20 mm diameter, 126 mg, respectively) and placed in an IR cell attached to a closed glass-circulation system. Prior to pyridine adsorption, the sample was dehydrated by heating at 300 °C for 1 h under vacuum. The intensity of the band at 1450 cm^{-1} (pyridine coordinatively bonded to Lewis acid sites) was plotted against the amount of pyridine adsorbed on the Lewis acid sites of the samples. The band intensity increased with the amount of chemisorbed pyridine and reached a plateau with the appearance of the band due to physisorbed pyridine (ca. 1440 cm^{-1}). While the band around 1440 cm^{-1} disappeared after evacuation at room temperature for 4 h, there was no significant difference in the intensity of the 1446 cm^{-1} band before and after evacuation, which indicated that the maximum intensity of the 1446 cm^{-1} band corresponded to the amount of Lewis acid sites available to chemisorb pyridine until saturation. The amount of Lewis acid sites on $BiPO_4$-DEG was estimated to be 26 μmol g^{-1} from the maximum band intensities and molecular absorption coefficient at 1446 cm^{-1}. The density of surface Bi cations on $BiPO_4$-DEG (D_{Bi}) was calculated to be 1.6 nm^{-2} from the BET surface area of $BiPO_4$-DEG (S_{BET}: 10 $m^2\ g^{-1}$) and the amounts of Lewis acid sites (A_L: 26 μmol g^{-1}) measured using pyridine-adsorbed IR. The equation is as follows: D_{Bi} (nm^{-2}) = N_A (Avogadro number: 6.02×10^{23} mol^{-1}) × A_L (mol g^{-1}) / S_{BET} ($m^2\ g^{-1}$) x $(10^9)^2$. For IR measurements with chloroform-adsorbed samples at 25 °C, a dehydrated sample (by heating at 300 °C for 1 h under vacuum) was exposed to chloroform vapor, and Fig. 8(c) shows IR spectra for $BiPO_4$-DEG at gas-phase chloroform pressures of 1.5×10^{-2} kPa, respectively. IR measurements with acetone and methanol-adsorbed samples at 25 °C were prepared by exposure of the dehydrated sample (by heating at 300 °C for 1 h under vacuum) to saturated acetone and methanol vapor followed by evacuation at 25 °C for 30 min to remove weakly physisorbed acetone and methanol.

Stable surface determination by DFT. First of all, we have performed the surface energy calculation of (100), (110), and (111) surfaces of $BiPO_4$ to identify the most stable surface structures, since these surfaces with low Miller index are expected to be exposed in the experimental condition of CH_4 activation. The surface energy is calculated as $E_{\mathrm{surf}} = 1/A(E_{\mathrm{slab}} - N \cdot E_{\mathrm{bulk}})/A$, where A is the surface area calculated from the slab unit cell, E_{slab} is the DFT energy of the slab, E_{bulk} is the DFT energy of the bulk $BiPO_4$, and N is the number of $BiPO_4$ bulk unit in the calculated slab model. The unit cells of the (100), (110), and (111) surfaces are shown in Fig. S5, and the calculated surface energies (in meV/Å^2) are also shown there. The calculated values have shown that (100) and the lowest surface energy (26.4 meV/Å^2), while (110) and (111) surface has higher energy (86.4 and 127.4 meV/Å^2, respectively). From these results, we can conclude (100) surfaces are expected to be exposed in the surface of $BiPO_4$ catalyst.

Next, we have analyzed the structure of the $BiPO_4$ (100) surface under the reaction environment. The CH_4 oxidation takes place at temperature (T) of 450-600 °C and total pressure (p) around 0.1 MPa with $p\mathrm{CH_4}:p\mathrm{O_2}:p\mathrm{N_2}$ = 2:2:6, therefore the oxidative atmosphere would lead the surface oxidation. To determine the surface structure at this reactive environment, we have employed the *ab initio* thermodynamics scheme i.e. evaluated the T, P-dependent surface energy of several oxidized (and non-oxidized) surfaces. The T, P-dependent O atom chemical potential (μ_{O}) is calculated as

$$\mu_{\mathrm{O}}(T,P) = \mu_{\mathrm{O}}(T,P^0) + \frac{1}{2}kT\ln\left(\frac{P}{P^0}\right).$$

Here we set $\mu_{\mathrm{O}}(T = 0, P = 0)$ as the half of the total energy of O_2 molecule. $\mu(T, P^0)$ corresponds to the temperature dependent part of μ_{O}. The total energy of O_2 and $\mu(T, P^0)$ are obtained from the references.[S9,S10] Using the T, P-dependent surface energy, we evaluated the surface energy of following surfaces with the DFT; non-oxidized $BiPO_4$, 0.25, 0.50, and 1.00 monolayer (ML) Bi-oxidized $BiPO_4$, and P-oxidized $BiPO_4$. Here, O-atom adsorbed either on surface Bi or P atoms and these are denoted as Bi-oxidized and P-oxidized surfaces, respectively. E_{surf} is evaluated referencing the non-oxidized surface i.e. setting E_{surf} of this surface as zero. The Fig. S6 summarizes the T-dependent surface energies. The O_2 pressure is fixed to 0.02 MPa, which is close to the experimental condition. The results have shown that 0.25 ML Bi-oxidized surface has the lowest surface energy at all the temperature regions. The second lowest surface energy is 0.50 ML, and 1.00 ML surface and P-oxidized surfaces are unstable with respect to the non-oxidized surface as they have positive surface energies. Considering these results, we could conclude that the CH_4 activation on the $BiPO_4$ (100) with 0.25 ML Bi-oxidized surface.

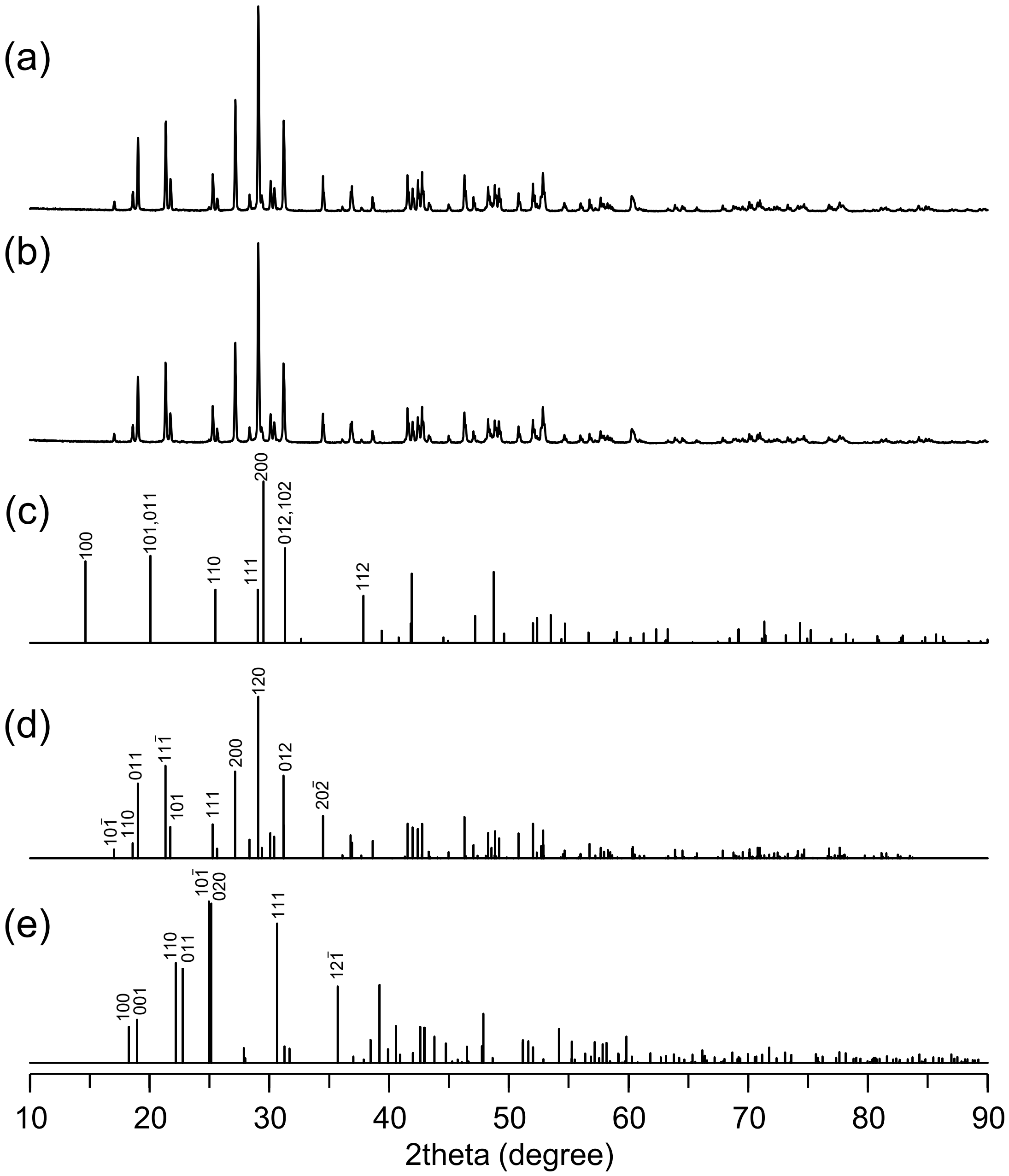

Fig. S1 XRD patterns for (a) $BiPO_4$-HT precursor, (b) $BiPO_4$-HT, (c) trigonal $BiPO_4 \cdot (H_2O)_{0.67}$ (ICSD 426233), (d) monoclinic $BiPO_4$ ($P2_1/n$, ICSD 426231), and (e) monoclinic $BiPO_4$ ($P2_1/m$, ICSD 426247).

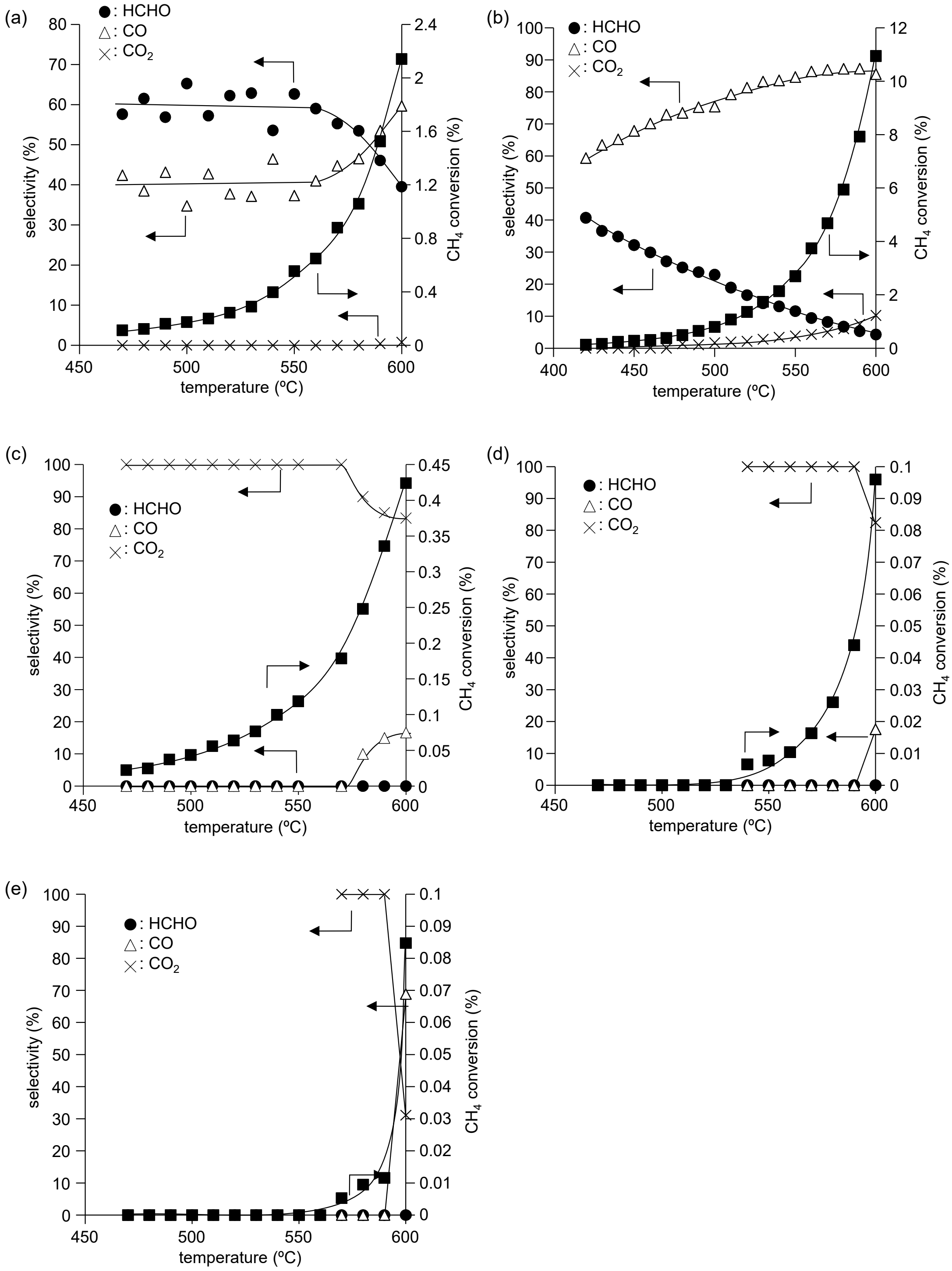

Fig. S2 Product selectivity and CH_4 conversion as function of reaction temperature with O_2 over the (a) $BiPO_4$-DEG, (b) $FePO_4$, (c) $BiPO_4$-HT, (d) α-Bi_2O_3, and (e) β-Bi_2O_3 catalysts. Reaction conditions: catalyst (100 mg), $CH_4/O_2/N_2$ (2/2/6 sccm), reaction temperature (420–600 °C).

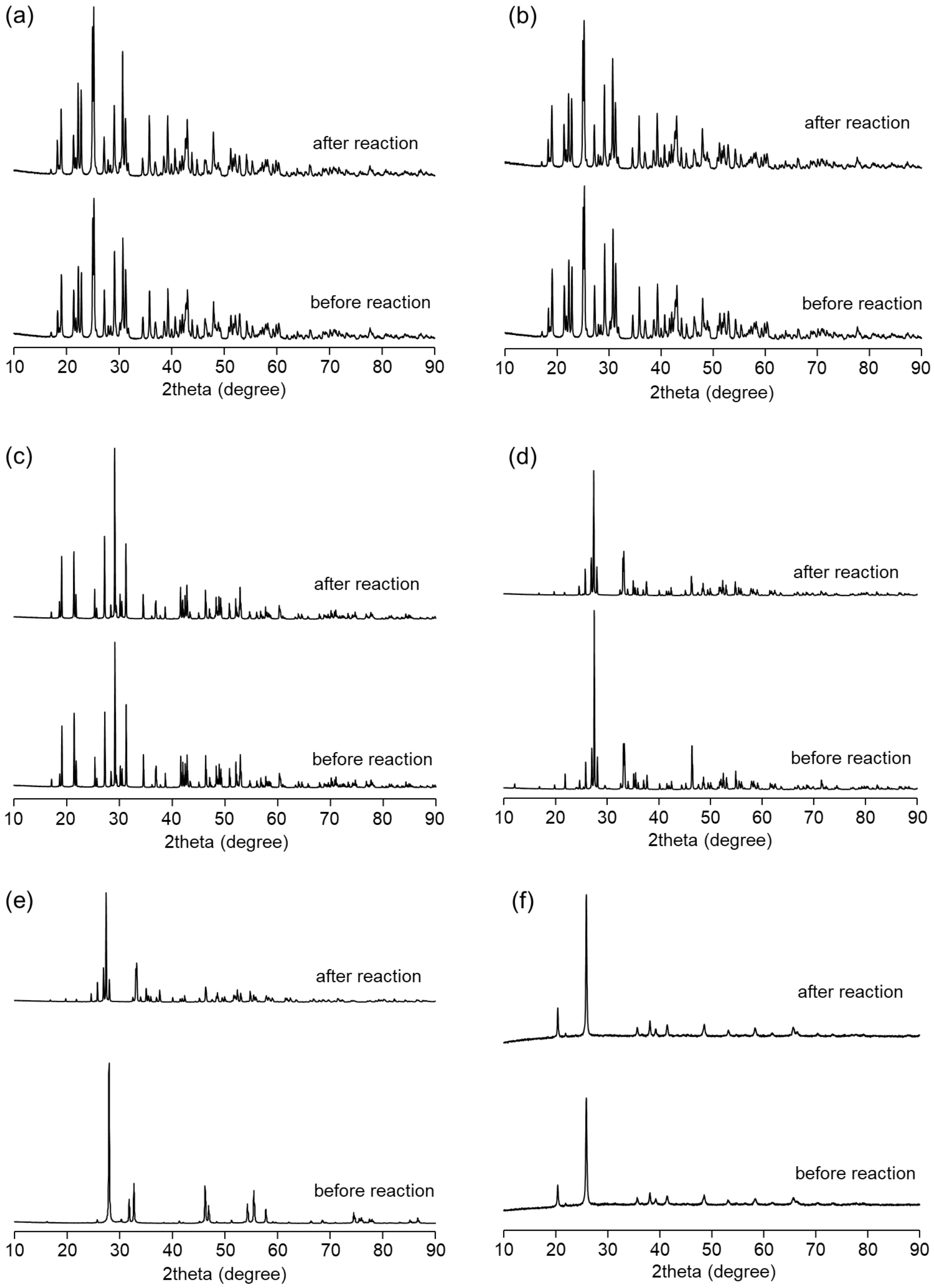

Fig. S3 XRD patterns for various catalyst before and after the oxidation of CH_4. (a) $BiPO_4$-DEG, (b) $BiPO_4$-DEG after time-on-stream experiments, (c) $BiPO_4$-HT, (d) α-Bi_2O_3, (e) β-Bi_2O_3, and (f) $FePO_4$. Reaction conditions are shown in Figs. 3 and S2.

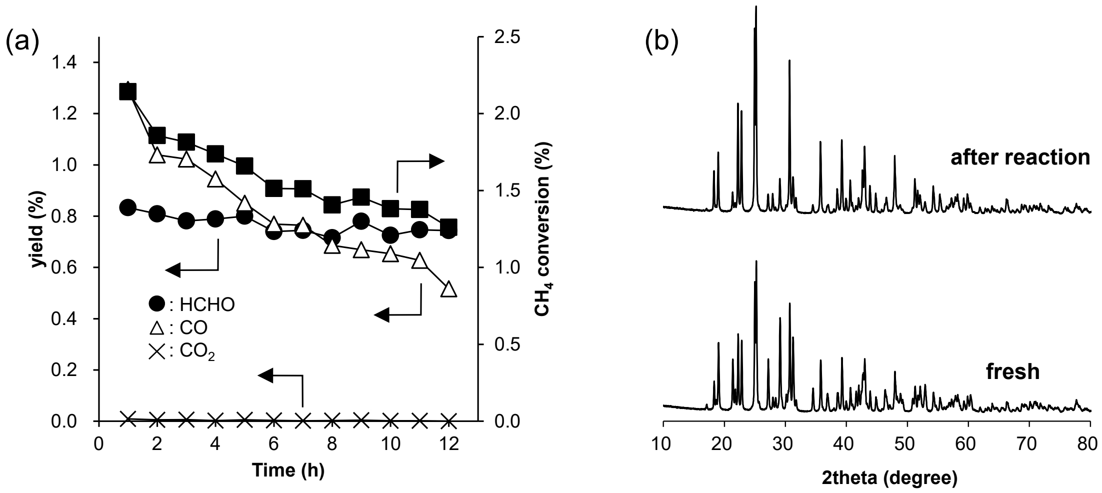

Fig. S4 (a) Time-on-stream performance of $BiPO_4$-DEG for oxidation of CH_4. Reaction conditions: $BiPO_4$-DEG (100 mg), $CH_4/O_2/N_2$ (2/2/6 sccm), 600 °C. (b) XRD patterns for BiPO4-DEG before and after the oxidation of CH_4 at 600 °C.

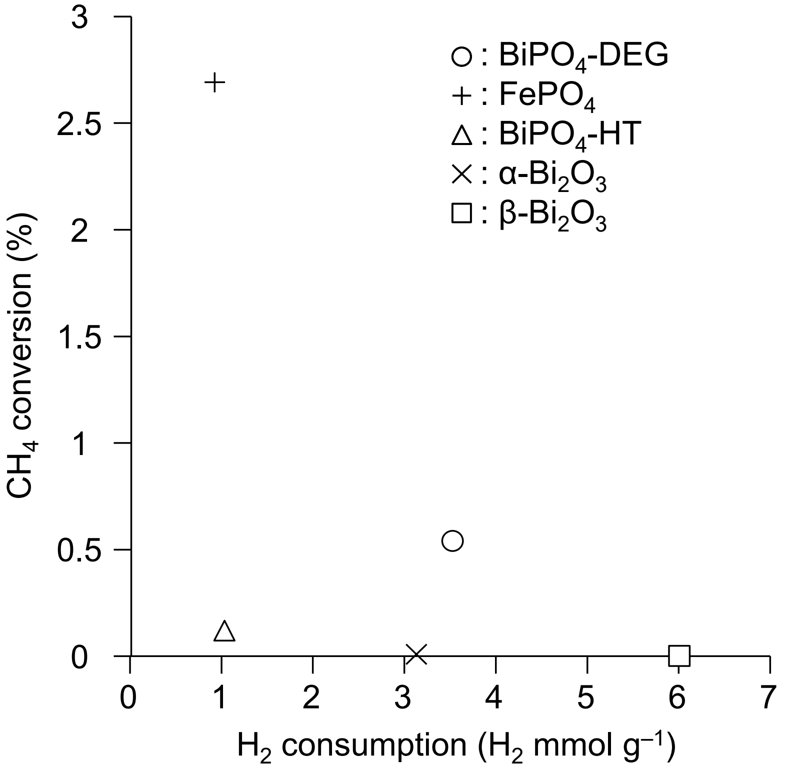

Fig. S5 CH_4 conversion at 550 °C for the oxidation of CH_4 with O_2 as function of H_2 consumption estimated by H_2-TPR analysis.

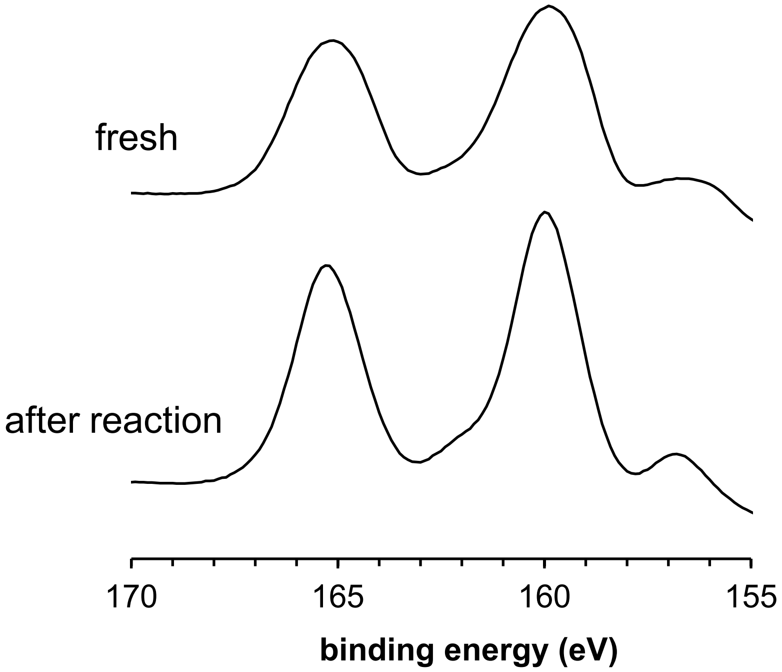

Fig. S6 Bi 4f XPS spectra $BiPO_4$-DEG before and after the oxidation of CH_4.

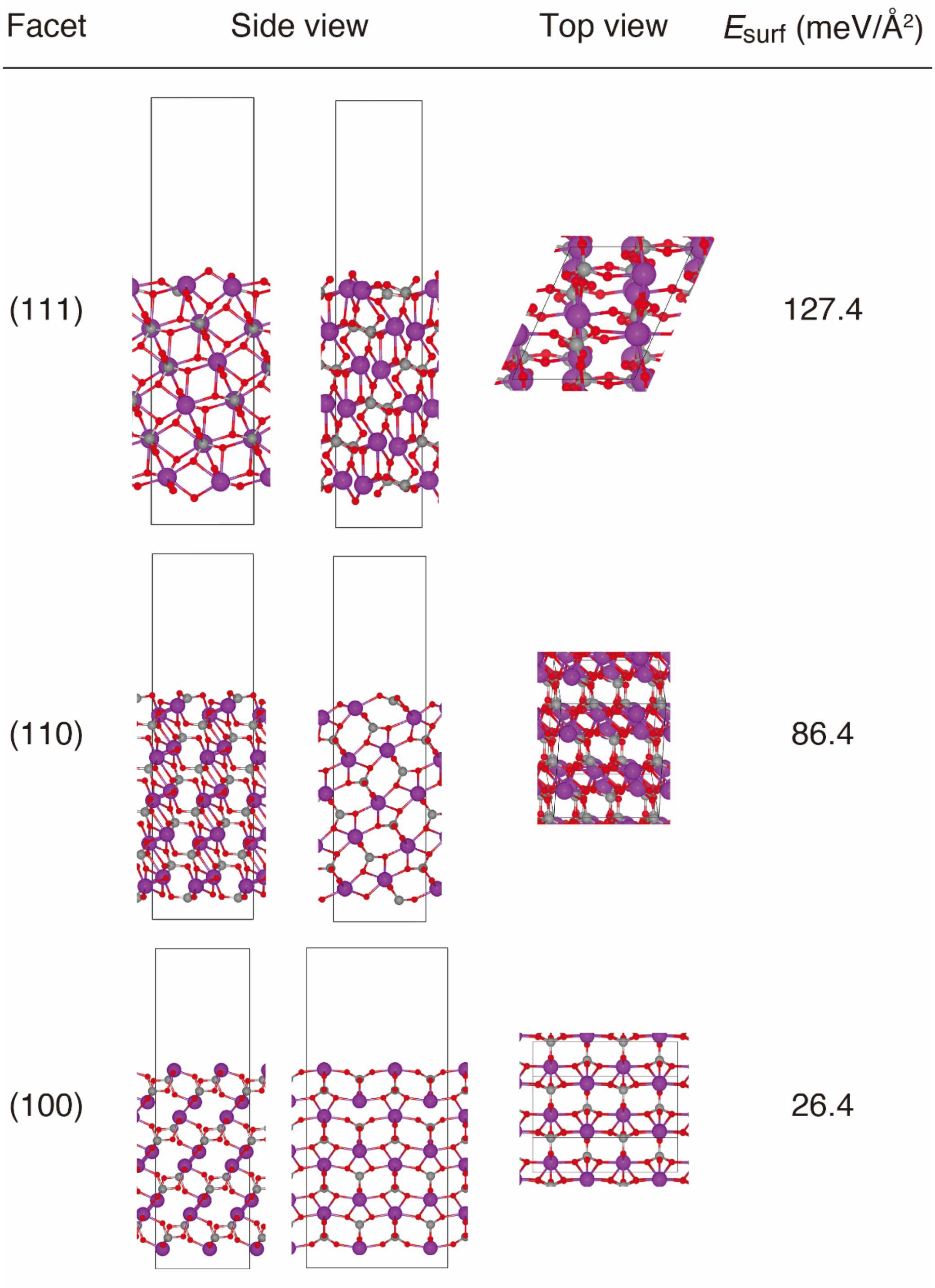

Fig. S7 Optimized geometries and surface energies (meV/Å^2) of (111), (110), and (100) surfaces of $BiPO_4$ calculated by the DFT. Bi, P, O atoms are represented by purple, gray, and red spheres, respectively. The solid line shows the boundary of the unit cell.

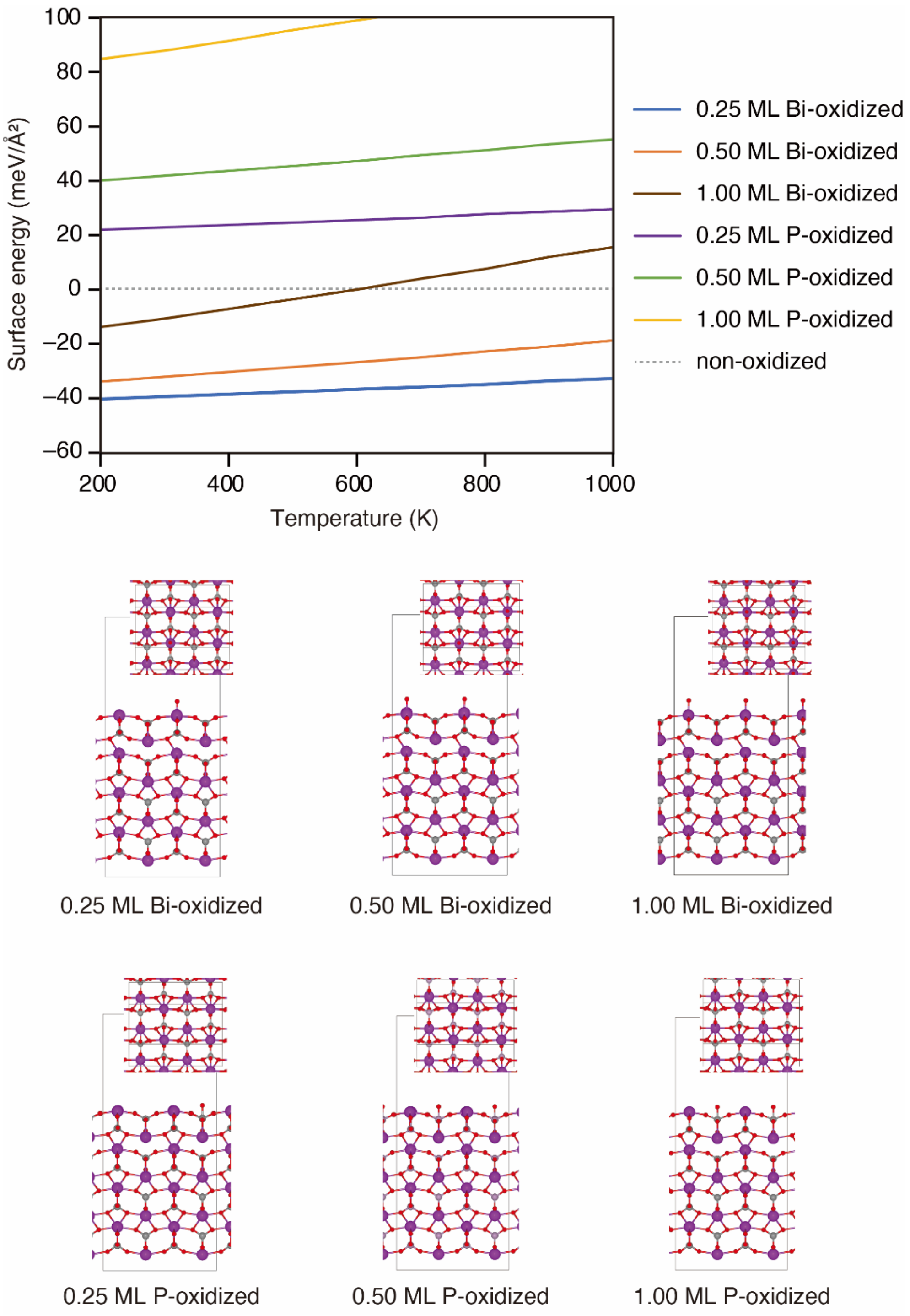

Fig. S8 Temperature-dependent surface energies of six oxidized and non-oxidized surface. The bottom panel shows the optimized structure of oxidized surfaces. The O_2 pressure is fixed to 0.02 MPa.

References

(S1) A. Matsuda, H. Tateno, K. Kamata and M. Hara, *Catal. Sci. Technol.*, 2021, **11**, 6987–6998.

(S2) Y. Yamaguchi, R. Aono, E. Hayashi, K. Kamata and M. Hara, *ACS Appl. Mater. Interfaces*, 2020, **12**, 36004–36013.

(S3) E. Hayashi, Y. Yamaguchi, K. Kamata, N. Tsunoda, Y. Kumagai, F. Oba and M. Hara, *J. Am. Chem. Soc.*, 2019, **141**, 890–900.

(S4) K. Kamata, K. Sugahara, Y. Kato, S. Muratsugu, Y. Kumagai, F. Oba, M. Hara, *ACS Appl. Mater. Interfaces*, 2018, **10**, 23792–23801.

(S5) K. Sugahara, K. Kamata, S. Muratsugu and M. Hara, *ACS Omega*, 2017, **2**, 1608–1616.

(S6) S. Kanai, I. Nagahara, Y. Kita, K. Kamata and M. Hara, *Chem. Sci.*, 2017, **8**, 3146–3153.

(S7) T. Komanoya, K. Nakajima, M. Kitano and M. Hara, *J. Phys. Chem. C*, 2015, **119**, 26540–26546.

(S8) K. Nakajima, Y. Baba, R. Noma, M. Kitano, J. N. Kondo, S. Hayashi and M. Hara, *J. Am. Chem. Soc.*, 2011, **133**, 4224–4227.

(S9) K. Reuter and M. Scheffler, *Phys. Rev. Lett.*, 2003, **90**, 046103.

(S10) W. Bergermayer, H. Schweiger and E. Wimmer, *Phys. Rev. B*, 2004, **69**, 195409.